Editors' Suggestion

Transmittable Nonreciprocal Cloaking

Mojtaba Dehmollaian,[1,*] Guillaume Lavigne,[1,†] and Christophe Caloz[2,‡]

[1] *Poly-Grames Research Center, Polytechnique Montréal, 2500 Chem. de Polytechnique, Montréal, Québec H3T 1J4, Canada*

[2] *ESAT-WaveCoRE-META Research Center, KU Leuven, Kasteelpark Arenberg 10, Leuven 3001, Belgium*

(Received 25 August 2022; revised 20 November 2022; accepted 8 December 2022; published 18 January 2023)

Cloaking is typically reciprocal. Here, we introduce the concept of *transmittable nonreciprocal cloaking*, whereby the cloaking system operates as a standard omnidirectional cloak for external illumination but can transmit light from its center outward at will. We demonstrate a specific implementation of such cloaking that consists of a set of concentric bianisotropic metasurfaces, the innermost element of which is nonreciprocal and designed to simultaneously block inward waves and pass—either omnidirectionally or directionally—outward waves. Such cloaking represents a fundamental diversification of conventional cloaking and may find applications in areas such as stealth, blockage avoidance, illusion, and cooling.

DOI: 10.1103/PhysRevApplied.19.014051

I. INTRODUCTION

Cloaking is a powerful concept in electromagnetics that emerged in 2006 as an outgrowth of metamaterials [1,2] and that has known vibrant and unabated development since that time [3]. A cloak is a metamaterial shell structure with medium properties that are designed so as to curve the trajectory of incident light around its core, the contents of which are hence made invisible to external observers. Different types of cloaking techniques have been reported, including coordinate-transformation deviation [2,4], scattering cancellation [5,6], transmission-line matching [7], gain compensation [8], and metasurface multiple scattering [9] or waveguiding [10].

The quasitotality of the cloaking structures reported to date is *reciprocal*: they fully satisfy the Lorentz reciprocity theorem [11]. Exceptions are the one-way cloaks presented in Refs. [12,13] and the unidirectional loss-and-gain balanced cloak presented in Ref. [14]. These devices perform cloaking for light incident from a given direction but reflect light incident from the opposite direction. They therefore represent *nonreciprocal* cloaks.

Here, we present a completely different type of nonreciprocal cloak. This device exhibits the property of *transmittable nonreciprocity*, operating as a standard—and hence also omnidirectional (contrary to Refs. [12–14])—cloak for external illumination, and as a transmission medium that is activable at will and that allows beam forming, for internal (core) illumination. It is implemented in the form of a set of concentric bianisotropic metasurfaces [15,16], with the innermost element being a nonreciprocal metasurface, which may be realized in magnetless transistor technology [17].

II. OPERATIONAL PRINCIPLE

Figure 1 provides a comparative description of the proposed transmittable nonreciprocal cloaking concept, with the usual cloaking shell structure and its core, the contents of which are made invisible, via light deviation, to external observers for external illumination.

Figure 1(a) depicts reciprocal cloaking. Waves (red arrows) impinging on the structure from an external source are bent by the cloaking shell around the core, A, which is hence made invisible to external observers B and C. While the figure represents an incident *plane wave*, with trivial angular spectrum $\delta(\vec{k}-\vec{k}_i)$, where $\vec{k}_i$ is the (fixed) incident wave vector, the cloaking effect occurs for *any type of wave* (e.g., a circular wave emitted by a close point source) and for any *incidence angle* (circular symmetry: $\theta_i \in [-\pi/2, \pi/2]$, or omnidirectionality). None of the rays forming the incident wave, whatever its nature, can penetrate into the core region, given its point-singularity origin. Therefore, in the absence of an external force and nonlinearity [18], light emitted from the core region would also not find any transmission channel through the cloaking shell and would hence be reflected from it, as illustrated in the figure (blue arrows). The system is thus fully reciprocal.

Figure 1(b) presents the proposed concept of *transmittable nonreciprocal cloaking*. The operation of the system is identical to that of the conventional cloak [Fig. 1(a)]

*mdehmollaian@gmail.com
†guillaume.lavigne@polymtl.ca
‡christophe.caloz@kuleuven.be

 © 2023 American Physical Society

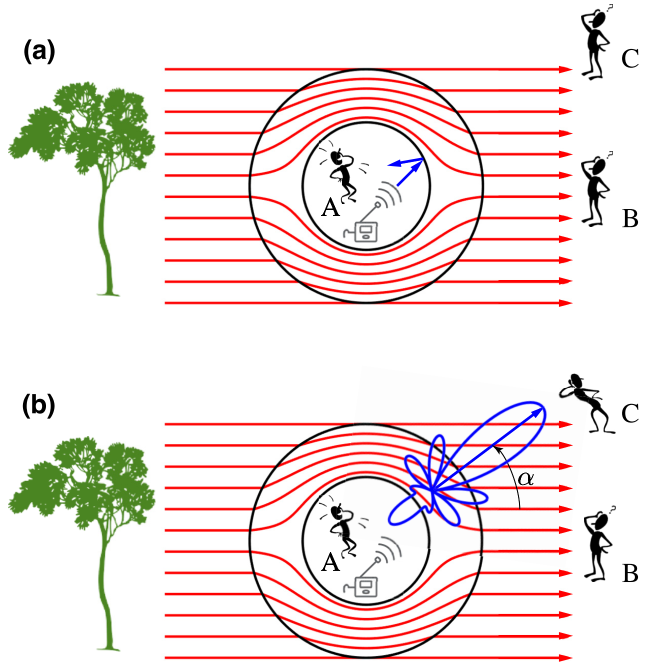

FIG. 1. A comparative description of transmittable nonreciprocal cloaking. (a) Conventional (reciprocal) cloaking, with invisibility for external illumination and reflection for internal illumination. (b) The proposed nonreciprocal cloaking, with conventional (omnidirectional) invisibility for external illumination and transmission—possibly directive—for internal illumination.

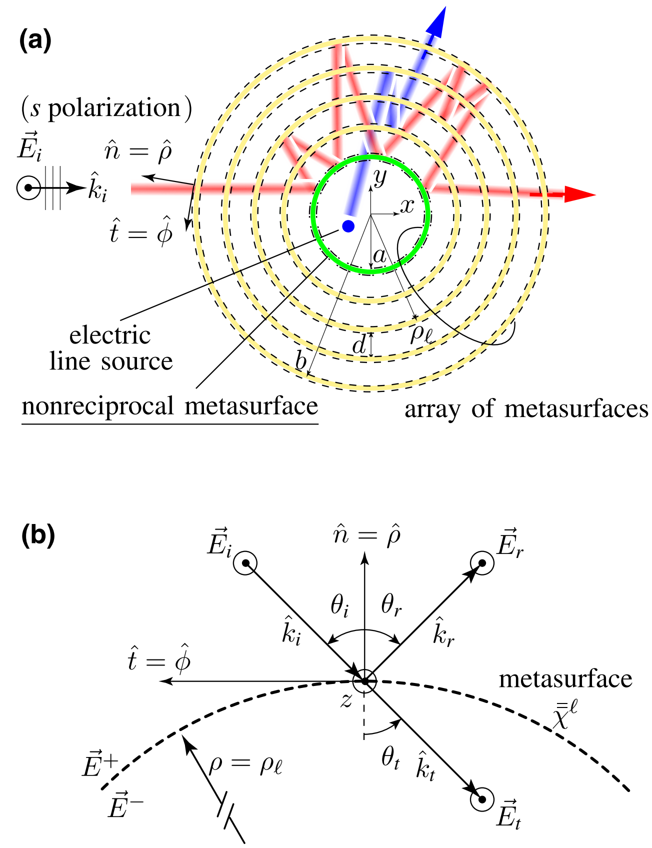

FIG. 2. The metasurface implementation of the transmittable nonreciprocal cloak in Fig. 1(b): (a) a concentric metasurface structure; (b) a curved metasurface sheet modeling any of the metasurfaces in (a).

for *external illumination*, i.e., the system cloaks its contents for any incident wave and incidence angle, making A invisible to observers B and C. However, instead of always reflecting light for *internal illumination*, the system can directionally *transmit* light through the shell outward to an intended external observer, C, who would then see either the background environment, as B, if A is silent, or a superposition of the background environment *and* a wave coming from the core of the system if A emits.

III. CONCENTRIC METASURFACE IMPLEMENTATION

The construction of a cloak, even a reciprocal one, is generally a challenging task. The most powerful cloaking technique—coordinate transformation—requires a complex voluminal inhomogeneous and anisotropic medium as well as unattainable infinite parameter values at the innermost boundary of the shell [2], while other cloaking techniques involve other well-documented difficulties along with specific limitations. On the other hand, both reciprocal [15] *and* nonreciprocal metasurfaces [17,19] have recently been demonstrated as practically viable electromagnetic devices. Therefore, here we select a metasurface-based approach for the implementation of the transmittable nonreciprocal cloak in Fig. 1(b).

Figure 2 describes the selected metasurface implementation structure. This structure, the reciprocal version of which has initially been suggested in Ref. [9], consists of a set of concentric uniform circular bianisotropic (gainless and lossless) metasurfaces, with the innermost element replaced by a nonreciprocal metasurface, as shown in Fig. 2(a). The overall assembly forms a multiple-scattering system akin to a circular (cylindrical or spherical) metasurface-enhanced multilayer Fabry-Perot resonator that is optimized for minimal scattering (maximal cloaking) and nonreciprocity (outward transmission), leveraging the great parametric diversity of the system, which includes an arbitrary magnitude and phase of the reflection (generally asymmetric) and transmission parameters at each of the metasurfaces as well as arbitrary interspacing between the metasurfaces. The detailed design procedure is presented in Sec. V A.

Given its circular cavity, bianisotropic interface, and radially nonuniform features, this Fabry-Perot structure seems too complex to admit a precise explanation of the cloaking operation in terms of simple physics. However, this operation may be qualitatively understood as optimal wave routing along the porous circular waveguides formed by the metasurfaces, as suggested in Fig. 2(a) and as is illustrated later in full-wave simulations [20]. Fortunately, the nonreciprocal operation does not add major complexity to the operation of the overall system. Indeed, as is seen in Sec. V, given the inner boundary location and inward penetrability of the nonreciprocal metasurface, the cloaking design is independent of the transmission design, while the transmission design only depends unrestrictedly on the cloaking design, with the related nonreciprocal metasurface design following standard transistor-loaded [17,19,21,22] or time-modulated [23,24] nonreciprocal metasurface technologies.

IV. METASURFACE MODELING

The metasurfaces constituting the transmittable nonreciprocal cloaking structure in Fig. 2(a) are generically represented, with relevant parameters, in Fig. 2(b). Here, we model these metasurfaces via the generalized sheet-transition conditions (GSTCs) [25–27], which are a generalization of the classical boundary conditions including bianisotropic surface polarization current densities [16]. In the modeling, it is assumed that the radii of curvature of the metasurfaces are large compared to the wavelength, so that locally, the incident waves see homogeneous flat sheets and hence there are negligible diffraction effects.

Assuming an s-polarization scenario (a two-dimensional problem), zero normal surface currents (for simplicity), and the harmonic time convention $e^{j\omega t}$, the GSTCs read (see Appendix A)

$$E_z^+ - E_z^- = jk_0\left(\chi_{\text{me}}^{\phi z} E_{z,\text{av}} + \eta_0 \chi_{\text{mm}}^{\phi\phi} H_{\phi,\text{av}}\right) \tag{1a}$$

and

$$H_\phi^+ - H_\phi^- = \frac{jk_0}{\eta_0}\left(\chi_{\text{ee}}^{zz} E_{z,\text{av}} + \eta_0 \chi_{\text{em}}^{z\phi} H_{\phi,\text{av}}\right), \tag{1b}$$

where the superscripts $\pm$ refer to the fields at $\rho = \rho_\ell^\pm$, just above and below the ℓth sheet, k_0 and η_0 are the free-space wave number and wave impedance, respectively, χ_{ee}^{zz}, $\chi_{\text{em}}^{z\phi}$, $\chi_{\text{me}}^{\phi z}$, and $\chi_{\text{mm}}^{\phi\phi}$ represent electric to electric, magnetic to electric, electric to magnetic, and magnetic to magnetic surface susceptibilities, respectively, and $E_{z,\text{av}} = (E_z^+ + E_z^-)/2$ and $H_{\phi,\text{av}} = (H_\phi^+ + H_\phi^-)/2$ denote the average electric and magnetic fields at the metasurface sheet, respectively. The susceptibilities χ_{ee}^{zz}, $\chi_{\text{em}}^{z\phi}$, $\chi_{\text{me}}^{\phi z}$, and $\chi_{\text{mm}}^{\phi\phi}$ correspond to the assumed s-polarization regime, with the electric field along $\hat{z}$ and the tangential magnetic field along $\hat{\phi}$; in the p-polarized case, the relevant susceptibilities, corresponding to the tangential electric field along $\hat{\phi}$ and the magnetic field along $\hat{z}$, would be $\chi_{\text{ee}}^{\phi\phi}$, $\chi_{\text{em}}^{\phi z}$, $\chi_{\text{me}}^{z\phi}$, and χ_{mm}^{zz}.

The ℓth metasurface is denoted by the same superscript, as indicated in Fig. 2, and, according to Eq. (1), the corresponding (s-polarization) susceptibility is written in the compact tensorial form

$$\bar{\bar{\chi}}^\ell = \chi_{\text{ee}}^{zz,\ell}\hat{z}\hat{z} + \chi_{\text{em}}^{z\phi,\ell}\hat{z}\hat{\phi} + \chi_{\text{me}}^{\phi z,\ell}\hat{\phi}\hat{z} + \chi_{\text{mm}}^{\phi\phi,\ell}\hat{\phi}\hat{\phi}, \tag{2}$$

where the four susceptibilities are constant, i.e., not functions of ϕ, according to the uniformity (or circular symmetry) assumption that ensures cloaking omnidirectionality.

V. CLOAK DESIGN

A. Overall procedure

We design the transmittable nonreciprocal cloak in Fig. 2(a) by successively optimizing the structure for cloaking in the external plane-wave illumination regime and for transmission in the internal point- or line-source illumination regime, based on the parametric setup shown in Fig. 3. This is accomplished by using the electromagnetic analysis tool established in Sec. V B, which, incorporating the bianisotropic susceptibility GSTC metasurface model presented in Sec IV, provides the exact electromagnetic fields everywhere in the system, while the optimization can be performed with any standard optimization tool.

The twofold cloaking-transmission optimization results in the determination of the $4L$ susceptibility parameters in Eq. (2), for a given core radius a and cloak radius b, assuming, for simplicity, uniform metasurface interspacing d. The cloaking optimization fully determines the susceptibility parameters of the metasurfaces $1, \ldots, L-1$ and some of the susceptibility parameters of the metasurface L, while the nonreciprocity optimization determines the remaining susceptibility parameters of the metasurface L.

The cloaking optimization consists in minimizing the scattering cross section of the overall structure and is

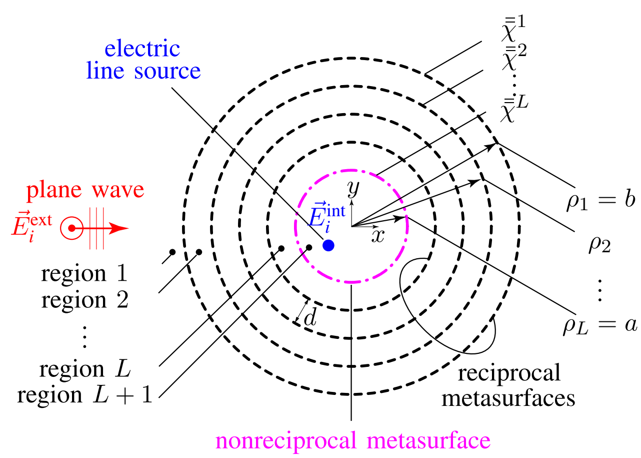

FIG. 3. The parametric setup for the design of the metasurface-based transmittable nonreciprocal cloak in Fig. 2(a).

detailed in Sec. V C, while the transmission optimization consists in adjusting the outward scattering parameters of the metasurface L and is detailed in Sec. V D. Both optimizations involve the scattering matrices of the different metasurfaces, where the scattering matrix of the ℓth metasurface is defined as $\mathbf{S}^\ell = [S_{11}^\ell, S_{12}^\ell; S_{21}^\ell, S_{22}^\ell]$ with port 1 corresponding to the region ℓ and port 2 corresponding to the region $\ell+1$, and with S_{ii}^ℓ being the reflection parameter at port i and S_{ij}^ℓ the transmission parameter from port j to port i $(i,j = 1,2)$ [16].

The cloaking and transmission designs, as set out in Sec. III, are essentially independent of each other, as far as the metasurfaces are concerned. Such independence is ensured by specifically making the Lth metasurface impenetrable to external illumination, i.e., by imposing $\left|S_{11}^L\right| = 1$, while subjecting the corresponding phase, $\angle S_{11}^L$, to cloaking optimization. In the internal-illumination regime, the cloaking-optimized globally transmissive nature of the metasurfaces $1,\ldots,L-1$ automatically provides an exit channel to the transmitted wave, while its radiation features may be independently controlled using antenna design principles. The case of simultaneous external and internal illumination is discussed in Sec. VI C.

B. Electromagnetic analysis

We analyze the system in Fig. 3 by successively expanding the metasurface-tangential fields in the different regions in cylindrical Bessel functions [28], applying the GSTCs in Eq. (1) at each metasurface interface between these regions [16], and resolving the resulting matrix system to obtain the expansion field coefficients.

The tangential electric and magnetic fields in the ℓth region can be expressed as

$$E_z^\ell = \sum_{n=-N}^{n=N} j^{-n}\left[b_n^\ell J_n(k_\ell\rho) + a_n^\ell H_n^{(2)}(k_\ell\rho)\right]e^{jn\phi} \qquad (3a)$$

and, from the Maxwell-Ampere equation,

$$H_\phi^\ell = \frac{1}{jk_\ell\eta_\ell}\frac{\partial E_z^\ell}{\partial\rho}, \qquad (3b)$$

where $J_n(\cdot)$ is the cylindrical Bessel function of the first kind, which accounts for multiple scattering within the annular and core regions, $H_n^{(2)}(\cdot)$ is the cylindrical Hankel function of the second kind, which accounts for radiation across the interfaces, k_ℓ and η_ℓ are the wave number and wave impedance of region ℓ, and a_n^ℓ and b_n^ℓ are the corresponding unknown expansion coefficients.

From this point, we enforce the GSTCs in Eq. (1) with the fields given in Eq. (3) at each metasurface boundary $(\ell = 1,2,\ldots,L)$ and match term by term $(n = -N,\ldots,N)$ the modal contributions of the resulting equations for the aforementioned external and internal illumination; this leads to a linear matrix system, the solutions of which are the field expansion coefficients a_n^ℓ and b_n^ℓ (see Appendix B).

C. Cloaking-regime scattering minimization

We make the following assumptions: (i) $\vec{E}_i^{\text{int}} = 0$ while $\vec{E}_i^{\text{ext}} \neq 0$, where $\vec{E}_i^{\text{int}}$ and $\vec{E}_i^{\text{ext}}$ are the external and internal incident fields, respectively (Fig. 3); (ii) all the metasurfaces are reciprocal, except for the innermost one $(\ell = L)$; (iii) all the metasurfaces are lossless and gainless, except for the innermost one (nonreciprocity implies some form of gain [18]); and (iv) the innermost region (region $L+1$) operates as a perfect electric conductor under external illumination—specifically, its permittivity is set to a very large negative imaginary number, to ensure impenetrability of the core of the cloak. The reciprocity condition implies that $\chi_{\text{em}}^{z\phi,\ell} = -\chi_{\text{me}}^{\phi z,\ell}$, while the gainless and lossless condition implies that $\chi_{\text{ee}}^{zz,\ell}$ and $\chi_{\text{mm}}^{\phi\phi,\ell}$ are purely real and $\chi_{\text{em}}^{z\phi,\ell} = -\chi_{\text{me}}^{\phi z,\ell}$ are purely imaginary [16].

We quantify the scattering of the structure under external illumination in terms of the scattering echo width [29], namely,

$$\delta(\phi) = \lim_{\rho\to\infty} 2\pi\rho\left|\frac{E^{\text{scat}}}{E^{\text{inc}}}\right|^2 = \frac{4}{k_0}\left|\sum_{n=-N}^{n=N} a_n^1 e^{jn\phi}\right|^2, \qquad (4)$$

where, in the last equality, we use the expression $E^{\text{scat}} = E_z^1$ for the field scattered in the unbounded $(b_n^1 = 0)$ medium 1 from Eq. (3a), apply the far-field approximation $H_n^{(2)}(k_\ell\rho\to\infty) = \sqrt{2/(\pi k_\ell\rho)}e^{-i(k_\ell\rho - n\pi/2-\pi/4)}$, and assume that the incident electric field is a plane wave with unit magnitude, i.e., $E^{\text{inc}} = E_{i,z}^{\text{ext}} = e^{-jk_0x}$.

The total scattering width, σ, which is the quantity to be minimized for cloaking, is then obtained upon integrating the echo width in Eq. (4) over all the scattering angles, as

$$\sigma = \frac{1}{2\pi}\int_0^{2\pi}\delta(\phi)d\phi = \frac{2}{\pi k_0}\int_0^{2\pi}\left|\sum_{n=-N}^{n=N} a_n^1 e^{jn\phi}\right|^2 d\phi. \quad (5)$$

For simplicity, we keep the innermost radius $(\rho_L = a)$, the spacing between the metasurfaces (d), the number of metasurfaces (L), the wave number (k_ℓ) and the wave impedance (η_ℓ) fixed for all values of ℓ and optimize only the bianisotropic susceptibility tensors $\bar{\bar{\chi}}^\ell$ $(\ell = 1,2,\ldots L)$. We perform this optimization iteratively, using an interior-point method, for the lowest normalized scattering width σ_{norm}, defined as the ratio of the total scattering width of the cloaked object [see Eq. (5)] to that of the innermost (impenetrable) circular metasurface. We thus solve the optimization problem

$$\min_{\bar{\bar{\chi}}^\ell} \sigma_{\text{norm}}\left(\bar{\bar{\chi}}^\ell, k_\ell, \eta_\ell, \rho_\ell, L\right) \qquad (6)$$

with a sufficiently large L to obtain a sufficiently small minimum σ_{norm} (e.g., $\sigma_{\text{norm}}^{\text{min}} = 10^{-3}$), under the scattering constraints

$$\left|S_{11}^{L}\right| = 1 \tag{7a}$$

and

$$\left|S_{21}^{L}\right| = 0, \tag{7b}$$

where $\angle S_{11}^{L}$ is a free design parameter. According to Eq. (1), these constraints imply the following conditions on the fields at the two sides of the Lth metasurface:

$$E_z^{+}=1+S_{11}^{L}, \quad E_z^{-}=0 \tag{8a}$$

and

$$H_\phi^{+}=\frac{1-S_{11}^{L}}{\eta_0}, \quad H_\phi^{-}=0, \tag{8b}$$

in which $S_{11} = e^{j\angle S_{11}}$ according to Eq. (7a), where a specific value is found for $\angle S_{11}$ at the end of the optimization procedure.

D. Transmission-regime beam forming

The illumination assumption is now $\vec{E}_i^{\text{ext}} = 0$, with $\vec{E}_i^{\text{in}} \neq 0$, and we impose the transmission constraints

$$\left|S_{22}^{L}\right| = 0 \tag{9a}$$

and

$$\left|S_{12}^{L}\right| = 1, \tag{9b}$$

which are naturally nonreciprocal in conjunction with Eq. (7), with $\angle S_{12}^{L}$ being a free design parameter that we arbitrarily set to zero. According to Eq. (1), these constraints imply the following conditions on the fields at the two sides of the Lth metasurface:

$$E_z^{+}=1,\ E_z^{-}=1, \tag{10a}$$

$$H_\phi^{+}=-\frac{1}{\eta_0},\ H_\phi^{-}=-\frac{1}{\eta_0}. \tag{10b}$$

E. Susceptibility parameters of the *L*th metasurface

Separately inserting Eqs. (8) (the external-illumination condition) and (10) (the internal-illumination condition) into Eq. (1) and solving the resulting system of four equations for the susceptibility parameters yields

$$\chi_{\text{ee}}^{zz,L} = \chi_{\text{em}}^{z\phi,L} = -\frac{j}{k_0}\left(1-S_{11}^{L}\right) \tag{11a}$$

and

$$\chi_{\text{me}}^{\phi z,L} = \chi_{\text{mm}}^{\phi\phi,L} = -\frac{j}{k_0}\left(1+S_{11}^{L}\right), \tag{11b}$$

where we recall that $S_{11} = e^{j\angle S_{11}}$, with $\angle S_{11}$ determined by the cloaking optimization (Sec. V C).

The relations in Eq. (11) fully determine the Lth metasurface, without omitting any *metasurface* degrees of freedom, beyond the essential conditions given in Eq. (10), for transmission optimization. However, this is not excessively constraining because (i) the cloaking-optimized globally transmissive nature of the metasurfaces 1 to $L-1$ automatically provides an exit channel to the transmitted wave and (ii) the radiation characteristics of this wave may be independently controlled using the antenna design principle, as is seen in Sec. VI.

VI. FULL-WAVE RESULTS

In this section, we consider a transmittable nonreciprocal cloak (Fig. 3) with a uniform metasurface spacing of $d = \lambda/4$ and a core radius of $\rho_L = \lambda$, where λ is the wavelength of the waves to be manipulated. Applying the design procedure outlined in Sec. V, using an interior-point optimization tool, we find that $N = 8$ metasurfaces are required to achieve $\sigma_{\text{norm}} < 10^{-3}$ under these conditions. In the following, we present the corresponding (full-wave) results, all of which are produced using the tools established in Sec. V.

Figure 4 shows the bianisotropic susceptibility parameters given by Eq. (2), obtained by means of the cloaking optimization in Sec. V C, for the metasurfaces 1 to $L-1$ and by Eq. (11) for the metasurface L, with the real and imaginary parts plotted in Figs. 4(a) and 4(b), respectively. Note that $\text{Re}\{\chi_{\text{em}}^{z\phi,\ell}\} = \text{Re}\{\chi_{\text{me}}^{\phi z,\ell}\} = \text{Im}\{\chi_{\text{ee}}^{zz,\ell}\} = \text{Im}\{\chi_{\text{mm}}^{\phi\phi,\ell}\} = 0$ and $\chi_{\text{em}}^{z\phi,\ell} = \chi_{\text{me}}^{\phi z,\ell}$ for $\ell = 1, 2, \ldots, 7$, according to the lossless-gainless and reciprocity specifications, respectively, whereas these conditions are violated in the $\ell = 8$th metasurface, according to the nonreciprocity specification and the related lossy condition [18]. The curves in Fig. 4 exhibit an overall trend of parameters increasing in magnitude from the outer to the inner layers of the system, as intuitively expected from the fact that deeper layers require stronger wave deviation for cloaking.

Figure 5 shows the scattering parameters corresponding to the susceptibilities in Fig. 4 under normal incidence, computed via conversion formulas provided in Ref. [16], with the magnitude and phase components plotted in Figs. 5(a) and 5(b), respectively.

Consistent with Fig. 5(a), the metasurfaces become progressively more reflective in the outer to inner direction of the structure, with the last metasurface being totally reflective and opaque from the exterior (i.e., $\left|S_{11}^{L}\right| = 1$

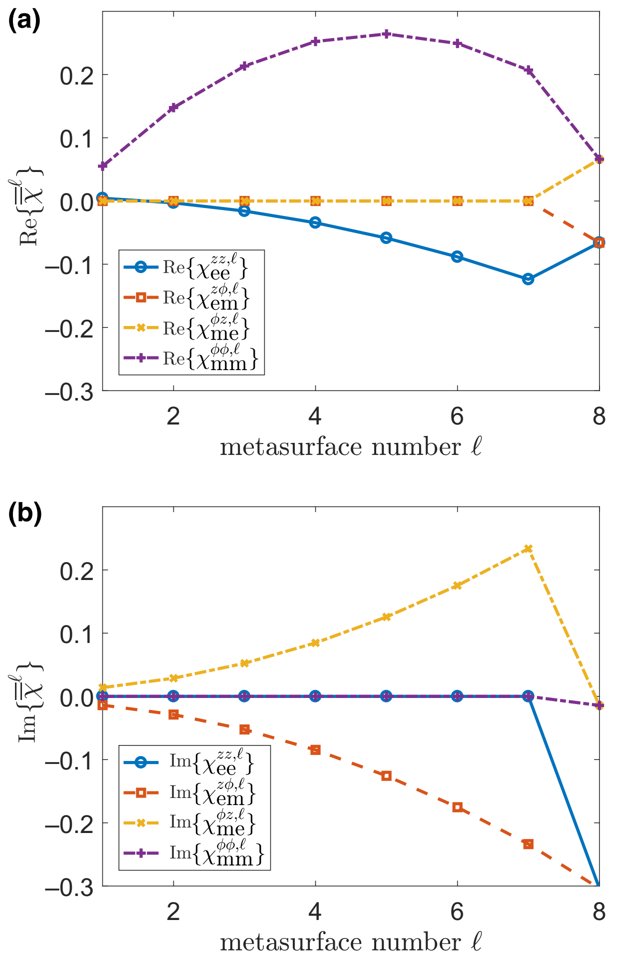

FIG. 4. The susceptibilities of the metasurfaces (in meters) for a transmittable nonreciprocal cloaking structure (Fig. 3) composed of $N = 8$ metasurfaces with uniform spacing $d = \lambda/4$ and with core radius $\rho_L = \lambda$: (a) real parts; (b) imaginary parts.

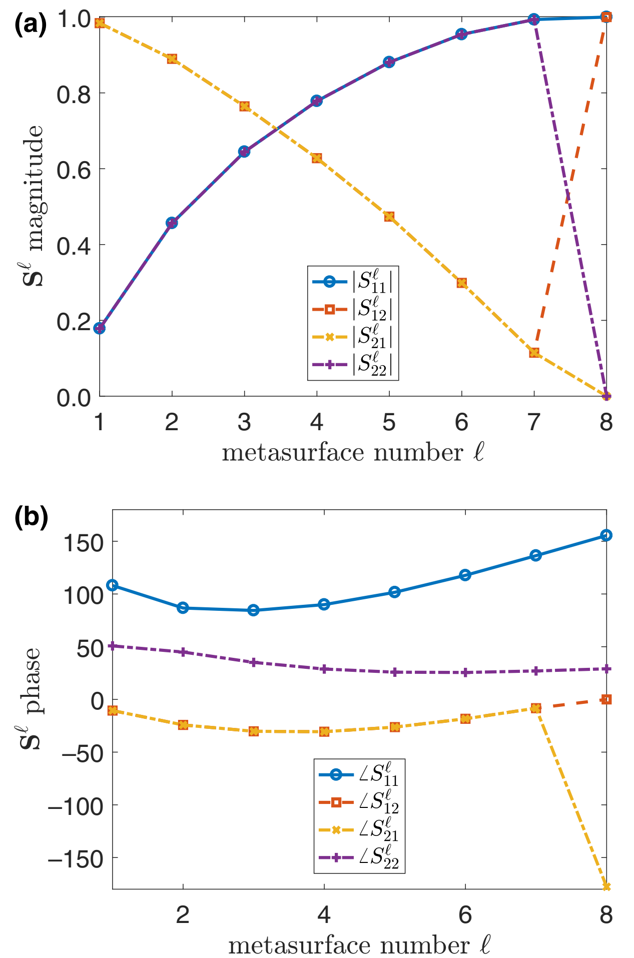

FIG. 5. The scattering parameters corresponding to the susceptibilities in Fig. 4 under normal incidence: (a) magnitude; (b) phase.

and $|S_{21}^L| = 0$) and perfectly matched and transmissive from the interior (i.e., $|S_{22}^L| = 0$ and $|S_{12}^L| = 1$). The result $\angle S_{11}^L \approx 155^\circ$ indicates that the innermost metasurface exhibits an external response that is fairly close but not exactly equal to that of a perfect electric conductor ($\angle S_{11} = 180^\circ$).

All the forthcoming results, up to the end of the paper, are obtained using the electromagnetic analysis presented in Sec. V B, based on optimized susceptibility results of the type in Fig. 4.

A. External illumination

Figure 6 presents the cloaking result under (external) plane-wave illumination, with Figs. 6(a) to 6(d) plotting the response of an impenetrable object without cloaking, for comparison, the response of the same object surrounded by the proposed cloak, the comparative responses of the two previous structures in a circular section of space, and the Poynting vector field corresponding to Fig. 6(b), respectively. Quasiperfect cloaking is observed. Note that the Poynting vector provides an insightful perspective on the multiple-scattering deviation mechanism in the concentric metasurface cloak structure, which, as may have been intuitively expected, is not so different from that of the coordinate-transformation deviation. Although the cloaking result is shown here for one angle, the device is a circularly symmetric structure, as previously mentioned, and hence it exhibits exactly the same cloaking performance for any angle of incidence (omnidirectional cloaking).

Figure 7 presents the cloaking result under (external) point- or line-source illumination. Here, again, a quasiperfect cloaking result is observed. This insensitivity of the structure to the nature of the source in cloaking may *a priori* seem surprising given that the cloak design is based on optimization under plane-wave incidence and not on a fundamental angle-independent scheme such as the coordinate-transformation one. The reason is that,

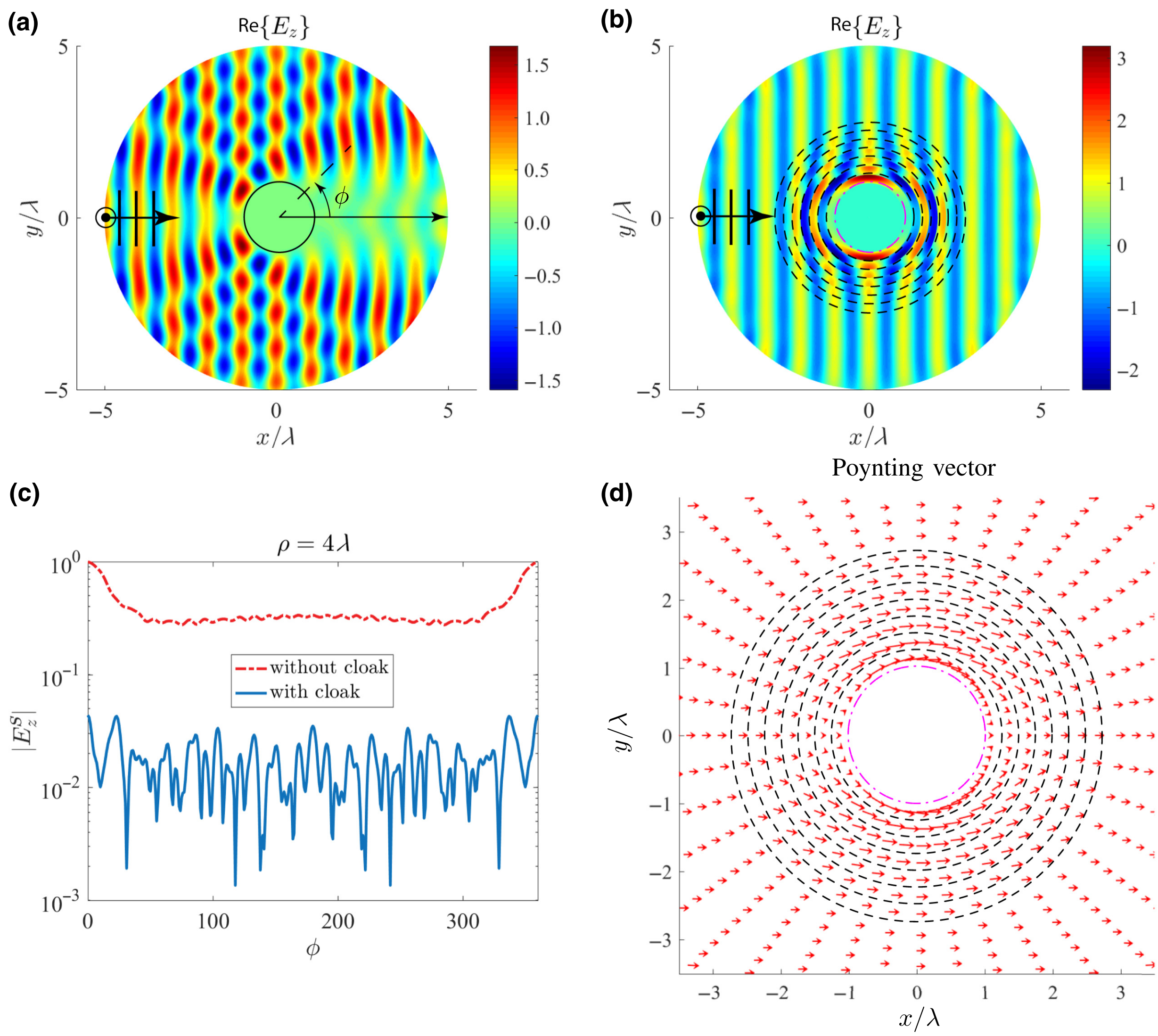

FIG. 6. Cloaking under (external) plane-wave illumination for the design in Figs. 4 and 5. (a),(b) The real part of the total electric field (in V/m) for (a) an impenetrable object without cloaking and (b) the same object surrounded by the proposed cloak. (c) The magnitude of the scattered field (in V/m) in (a) and (b) in the circular section $\rho = 4\lambda$. (d) The Poynting vector corresponding to (b).

although the plane wave impinges normally ($\phi = 0^\circ$) onto the equator of the cloak, it impinges on the latitudes from the equator to the poles with a continuum of all possible incidence angles ($\phi = 0^\circ \rightarrow 90^\circ$). Therefore, the optimization process automatically accounts for all the directions included in the angular spectrum of the point source (or any other source) and hence the cloak is working for any source topology.

B. Internal illumination

As pointed out in Sec. II and illustrated in Fig. 1(a), in a properly designed reciprocal cloak, light launched from the core of the device should essentially be reflected back by the cloak shell. Figure 8, which displays the response of the system under internal illumination with nonreciprocity turned off, shows that the selected concentric metasurface cloaking technique indeed exhibits this characteristic in the absence of nonreciprocity. The light confinement in the core is not perfectly clear, with the negligible leakage beyond the cloak shell (approximately 50 dB below the average core field) due to the imperfections in the design ($\sigma_{\text{norm}} \approx 10^{-3} \neq 0$).

Finally, Fig. 9 demonstrates the unique outward transmission capability of the proposed nonreciprocal cloak, with Figs. 9(a) and 9(b) showing omnidirectional transmission from a centered isolated source and directional transmission (with a directivity of 7.67 dB) from an offset mirror-backed source, respectively. As anticipated in Sec. II, the globally transmissive cloaking-optimized structure beyond the innermost (nonreciprocal) metasurface provides a proper exit channel to the wave originating from

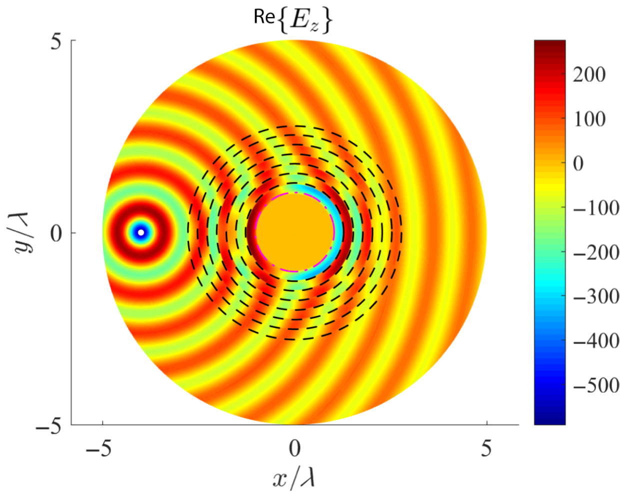

FIG. 7. Cloaking under (external) point- or line-source illumination for the design in Figs. 4 and 5 (the real part of the total electric field in V/m), with the source placed at the point $\rho = 4\lambda$ and $\phi = \pi$ (see Fig. 3).

the core of the cloak. In fact, more sophisticated designs, still independent of the cloaking design or codesigned with it, could be achieved, such as higher-directivity radiation and advanced beam forming, using an array of a few antenna elements following standard antenna-design techniques [30].

C. Simultaneous external and internal illumination

The proposed transmittable nonreciprocal cloak may operate either in "simplex mode," whereby either only the cloaking operation [$\vec{E}_i^{\text{ext}} \neq 0$ but $\vec{E}_i^{\text{int}} = 0$ (silent transmitter)] or the transmitting function [$\vec{E}_i^{\text{int}} \neq 0$ but $\vec{E}_i^{\text{ext}} = 0$ (nonilluminated cloak)] is active at a given time, as illustrated in Figs. 6(b) and 7 for the former case and Fig. 9 for the latter case. However, it is especially designed to operate in "full-duplex mode" [$\vec{E}_i^{\text{ext}} \neq 0$ and $\vec{E}_i^{\text{int}} \neq 0$], where the two operations are performed simultaneously. This scenario is illustrated in Fig. 10. This figure, which naturally corresponds to a superposition of the separate illumination results given the linearity of the overall system, provides a visual sense of the duplex operation of the system, whereby transmission is effectively produced in the intended direction while cloaking is realized everywhere else. Note that information carried by the transmitted wave could be easily received, despite the presence of the external source, using proper communication-modulation techniques [31].

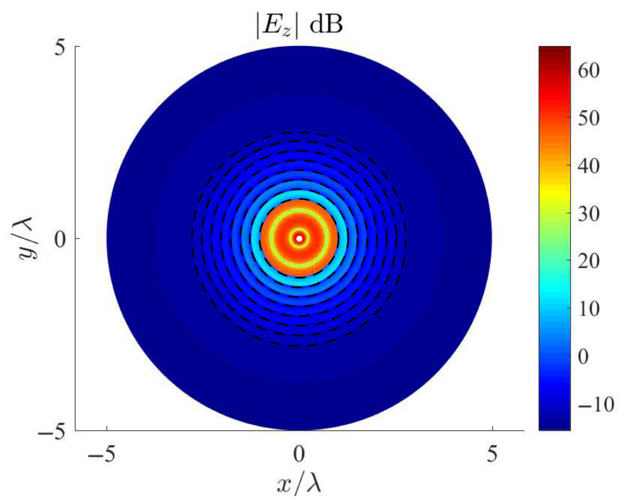

FIG. 8. The response of the structure with the design in Figs. 4 and 5 (the magnitude of the total electric field in dBV/m) under internal illumination (with a point source at the center) with nonreciprocity turned off.

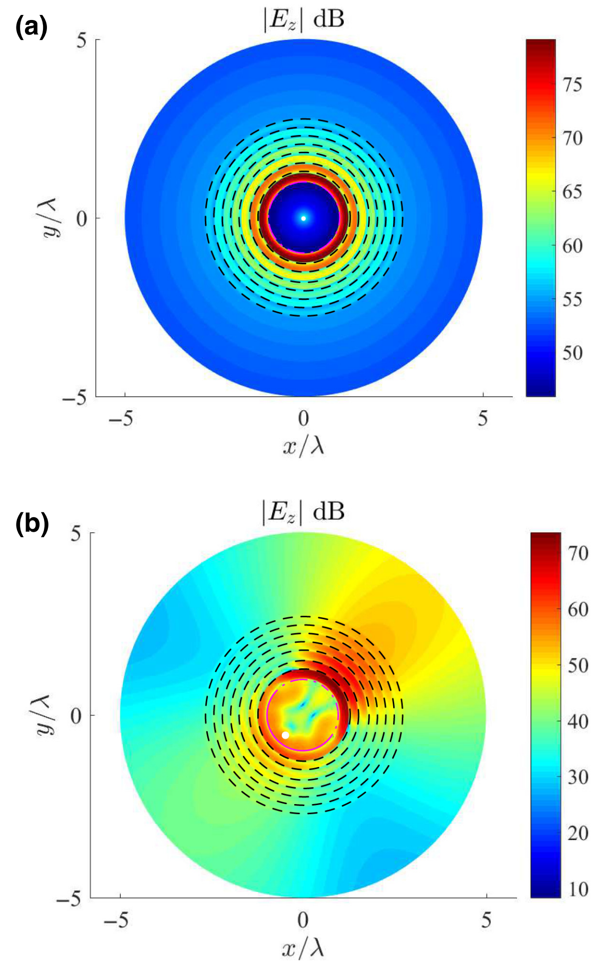

FIG. 9. Transmission under internal illumination for the design in Figs. 4 and 5 (the magnitude of the total electric field in dBV/m) with nonreciprocity turned on. (a) An omnidirectional (point) source placed at the center of the structure. (b) Directive radiation toward $\alpha = 45^{\text{o}}$, with the point source placed at $(\rho', \phi') = (3\lambda/4, 5\pi/4)$ and backed by a half-circular reflector.

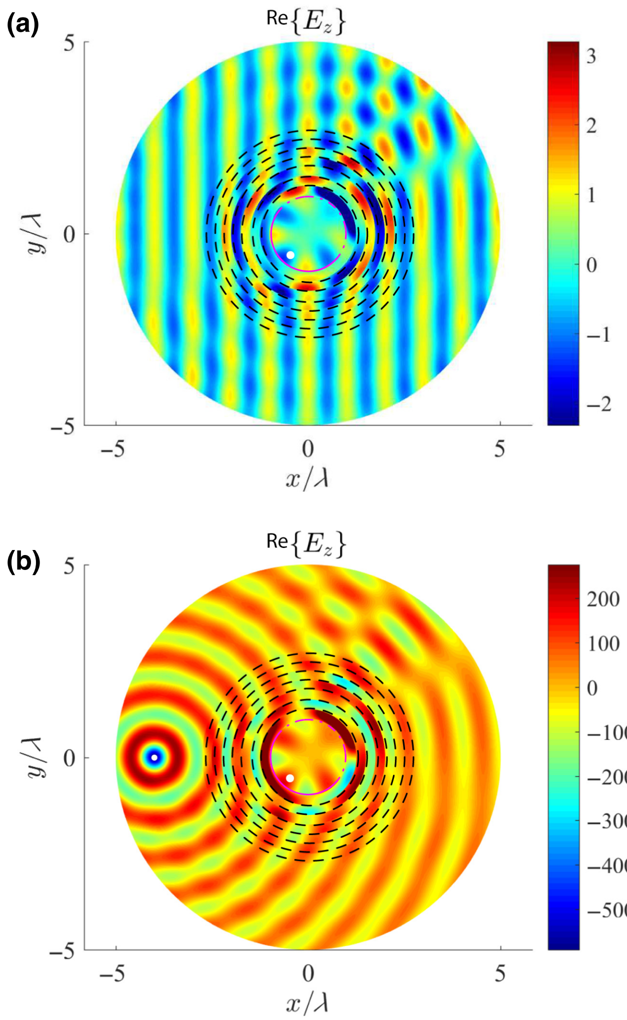

FIG. 10. The response of the transmittable nonreciprocal cloak under simultaneous external and internal illumination (the real part of the total electric field in V/m) for an internal point or line source located at $(3\lambda/4, 5\pi/4)$ and (a) an external plane-wave source with wave amplitude unity along with an internal source of 0.002 A and (b) an external point- or line-source strength of 1 A at $(4\lambda, \pi)$, along with an internal point- or line-source strength of −0.25 A.

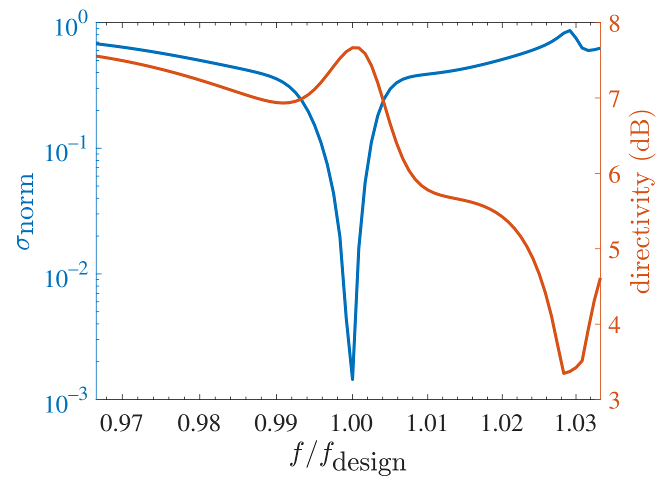

FIG. 11. The frequency response of the nonreciprocal transmittable cloak in terms of the (normalized) scattering width [Eq. (5)] for external illumination (cloaking), with the parameters in Fig. 6(b), and directivity for internal illumination (transmission), with the parameters in Fig. 9(b).

D. Bandwidth considerations

Figure 11 plots the frequency response of the nonreciprocal transmittable cloak in both the cloaking and transmission regimes. The bandwidth of the system involves two aspects: (i) the bandwidth of the (Lorentz-type) resonant particles forming the metasurfaces and (ii) the bandwidth of the overall circular Fabry-Perot resonator structure, assuming unlimited-bandwidth metasurface particles. The bandwidth of the latter is bounded by the Fabry-Perot etalon layer having the most reflective interfaces, since the bandwidth of a Fabry-Perot etalon is inversely proportional to the product of its interface reflectances [BW $= 2/\mathcal{F}$, with finesse $\mathcal{F} = \pi\sqrt{|r_1 r_2|}/(1 - |r_1 r_2|)$] [32]. This typically corresponds to the innermost layer of the cloaking structure, as illustrated in Fig. 5(a); in this design, the reflectance product is 0.99, which yields a bandwidth of about 0.6%, consistent with the bandwidth of both the cloaking and transmission curves in Fig. 11. On the other hand, the bandwidth of resonant particles, which essentially depends on their specific geometries, is typically in the order of 5% [16]; this is one order of magnitude larger than the aforementioned Fabry-Perot resonance and therefore the metaparticle bandwidth limitation does not impact the bandwidth of the overall system.

VII. POTENTIAL APPLICATIONS

In this section, we describe some of the potential applications of the proposed transmittable nonreciprocal cloaking (Fig. 2).

A. Selective cloaking

As with any cloaking system, the proposed device may be used for camouflaging from radar, since the interrogating wave is deviated by the cloak around the object placed in its core without any reflection, as well as without scattering, which could be detected by a foe in a different location. However, this device offers the extra functionality of *camouflaging selectivity*, whereby the host of the cloak can communicate with friends while being undetectable by foes. This may be accomplished in two ways. If the position of the friend is known, one may use the directional option in Fig. 9(b) and possibly even rotate the antenna system (mechanically or electronically) to follow this friend or to reach other friends in different directions. If the position of the friend(s) is unknown, one may use the omnidirectional mode in Fig. 9(a) along with a spread-spectrum encryption key, so that the transmitted signal is spread out to a level below the noise floor of the foe but can be restored by the friend(s) upon multiplication with the encryption key in their possession [33].

B. Blockage avoidance

The feed of a parabolic antenna should ideally be dimensionless to avoid perturbing, by blockage and diffraction, the waves reflected by the parabolic dish. Unfortunately, the feed must have a size that is comparable to the wavelength for efficient radiation—and even substantially larger than the wavelength when over-spilling constraints require high feed directivity. The proposed device can resolve this issue in the antenna transmission mode. Indeed, placing the feed in the core of the nonreciprocal (omnidirectional) cloak allows the signal to radiate across the cloak so as to illuminate the dish, while the waves subsequently reflected by the dish are deviated around the feed via cloaking. This scheme would not readily work in the antenna receiving mode, where the received signal would be appropriately deviated by cloaking around the feed but could not then penetrate inside the cloak to reach the feed (two equivalent external sources); in that case, a simple solution would be to use a half (reciprocal) cloak, with the cloak side, of course, oriented toward the incidence side and the dish side left empty.

C. Electromagnetic illusion

Electromagnetic (or optical) illusion has been mostly realized by the transformation-coordinate technique so far [34]. Given its greater fabrication simplicity and bianisotropic flexibility (36 accessible parameters [16]), the proposed metasurface-based cloaking approach has the potential for more diverse illusion operations. Moreover, the proposed nonreciprocity functionality could further enrich the illusion efficacy by having the entity in the core of the cloak launching strong deceptive signals, possibly with elaborate space-time spectral transformations [35].

D. Cooling window

Significant efforts have been made in recent years to realize smart windows that optimize thermal radiation in order to save energy [36]. An ideal window of that type would—e.g., in the summer, to save cooling energy—transmit indoor heat outward while reflecting outdoor (solar and environmental) heat, a clearly nonreciprocal operation that would benefit from nonreciprocal metasurfaces [17,21] operating at the appropriate infrared and far-infrared wavelengths. In this area, the additional cloaking feature of the proposed device, which might be implemented in windows of various (curved) shapes, might offer further thermal control flexibility in the near future.

VIII. CONCLUSION

We introduce the concept of transmittable nonreciprocal cloaking and demonstrate it by means of a concentric metasurface structure. This metasurface represents a fundamental diversification of the already powerful concept of cloaking and has potential applications, some of which have been described in Sec. VII.

APPENDIX A: METASURFACE MODELING

Assuming, for simplicity, a metasurface involving only *tangential* electric and magnetic surface-polarization densities, the GSTCs read as follows [37] [see Fig. 2(b)]:

$$\hat{\rho} \times \Delta\vec{E} = -j k_0 \eta_0 \vec{M}_{s,\parallel}, \tag{A1a}$$

$$\hat{\rho} \times \Delta\vec{H} = j\omega \vec{P}_{s,\parallel}, \tag{A1b}$$

where $\hat{\rho}$ is the unit vector normal to the surface of the metasurface, Δ refers to the difference of the fields (electric $\vec{E}$ and magnetic $\vec{H}$) on both sides of the metasurface at $\rho = \rho_\ell^-$ and $\rho = \rho_\ell^+$ (e.g., $\Delta\vec{E} = \vec{E}^+ - \vec{E}^-$), k_0 and η_0 are the free-space wave number and wave impedance, respectively, ω is the angular frequency, and $\vec{M}_{s,\parallel}$ (A) and $\vec{P}_{s,\parallel}$(C/m) are the tangential surface-magnetic and electric polarization densities, respectively, with the symbol $\parallel$ denoting vector components tangential to the metasurface.

In this model, $\vec{M}_{s,\parallel}$ and $\vec{P}_{s,\parallel}$ are expressed in terms of the susceptibility tensors $\bar{\bar{\chi}}_{\text{ee}\parallel}$, $\bar{\bar{\chi}}_{\text{em}\parallel}$, $\bar{\bar{\chi}}_{\text{me}\parallel}$, and $\bar{\bar{\chi}}_{\text{mm}\parallel}$, and in terms of the average electric and magnetic fields at the metasurface sheet [i.e., $\vec{E}_{\text{av}} = (\vec{E}^+ + \vec{E}^-)/2$ and $\vec{H}_{\text{av}} = (\vec{H}^+ + \vec{H}^-)/2$], i.e.,

$$\vec{M}_{s,\parallel} = \frac{1}{\eta_0}\bar{\bar{\chi}}_{\text{me}\parallel} \cdot \vec{E}_{\parallel,\text{av}} + \bar{\bar{\chi}}_{\text{mm}\parallel} \cdot \vec{H}_{\parallel,\text{av}}, \tag{A2a}$$

$$\vec{P}_{s,\parallel} = \epsilon_0 \bar{\bar{\chi}}_{\text{ee}\parallel} \cdot \vec{E}_{\parallel,\text{av}} + \frac{1}{c}\bar{\bar{\chi}}_{\text{em}\parallel} \cdot \vec{H}_{\parallel,\text{av}}, \tag{A2b}$$

where ϵ_0 and c are the free-space permittivity and the speed of light, respectively. In the problem at hand (see Fig. 2), where the fields are s polarized, the only contributing susceptibilities in Eq. (A2) are

$$\bar{\bar{\chi}}_{\text{ee}\parallel} = \chi_{\text{ee}}^{zz}\,\hat{z}\hat{z}, \tag{A3a}$$

$$\bar{\bar{\chi}}_{\text{em}\parallel} = \chi_{\text{em}}^{z\phi}\,\hat{z}\hat{\phi}, \tag{A3b}$$

$$\bar{\bar{\chi}}_{\text{me}\parallel} = \chi_{\text{me}}^{\phi z}\,\hat{\phi}\hat{z}, \tag{A3c}$$

$$\bar{\bar{\chi}}_{\text{mm}\parallel} = \chi_{\text{mm}}^{\phi\phi}\,\hat{\phi}\hat{\phi}. \tag{A3d}$$

The GSTCs in Eq. (1) are then obtained by substituting Eq. (A3) into Eq.(A2), and then inserting the resulting equations into Eq. (A1).

APPENDIX B: SCATTERING ANALYSIS

First, we expand the tangential fields in each layer ℓ, E_z^ℓ and H_ϕ^ℓ, over the natural modes of the system, which are Bessel functions in the radial direction, ρ, multiplied by the complex exponential function in the azimuthal direction, ϕ, namely,

$$E_z^\ell = \sum_{n=-N}^{n=N} j^{-n}\left[b_n^\ell J_n(k_\ell\rho) + a_n^\ell H_n^{(2)}(k_\ell\rho)\right] e^{jn\phi} = \sum_{n=-N}^{n=N} \tilde{E}_n^\ell(\rho)\, e^{jn\phi} \tag{B1a}$$

and

$$H_\phi^\ell = \frac{1}{jk_\ell\eta_\ell}\frac{\partial E_z^\ell}{\partial\rho} = \sum_{n=-N}^{n=N} \tilde{H}_n^\ell(\rho)\, e^{jn\phi}, \tag{B1b}$$

where we write the expansions in the convenient form of Fourier series, the spectral coefficients of which, $\tilde{E}_n^\ell$ and $\tilde{H}_n^\ell$, depend on ρ and explicitly read

$$\tilde{E}_n^\ell(\rho) = j^{-n}\left[b_n^\ell J_n(k_\ell\rho) + a_n^\ell H_n^{(2)}(k_\ell\rho)\right] \tag{B2a}$$

and

$$\tilde{H}_n^\ell(\rho) = \frac{j^{-(n+1)}}{\eta_\ell}\left[b_n^\ell J_n'(k_\ell\rho) + a_n^\ell H_n^{(2)\prime}(k_\ell\rho)\right]. \tag{B2b}$$

Then, we express the susceptibility parameters of each metasurface in terms of Fourier series, for later matching with the fields, i.e.,

$$\chi_{pq}^\ell(\phi) = \sum_{n=-2N}^{n=2N} \tilde{\chi}_{ab,n}^\ell\, e^{jn\phi}, \tag{B3a}$$

with the spectral coefficients

$$\tilde{\chi}_{pq,n}^\ell = \frac{1}{2\pi}\int_0^{2\pi} \chi_{ab}^\ell(\phi)\, e^{-jn\phi} d\phi, \tag{B3b}$$

where $p, q = e, m$, corresponding to the four nonzero susceptibilities $\chi_{\text{ee}}^{zz,\ell}$, $\chi_{\text{em}}^{z\phi,\ell}$, $\chi_{\text{me}}^{\phi z,\ell}$, and $\chi_{\text{mm}}^{\phi\phi,\ell}$, and where we drop the superscripts zz, $z\phi$, ϕz, and $\phi\phi$ for conciseness.

Finally, we apply the mode-matching technique at each metasurface boundary, $\rho = \rho_\ell$, in Fig. 3, by inserting Eqs. (B1) and (B3) into Eq. (1). This yields

$$\Delta\tilde{E}_n^\ell = jk_0\left(\tilde{\chi}_{\text{me},n}^\ell * \tilde{E}_{\text{av},n}^\ell + \eta_0\tilde{\chi}_{\text{mm},n}^\ell * \tilde{H}_{\text{av},n}^\ell\right) \tag{B4a}$$

and

$$\Delta\tilde{H}_n^\ell = j\frac{k_0}{\eta_0}\left(\tilde{\chi}_{\text{ee},n}^\ell * \tilde{E}_{\text{av},n}^\ell + \eta_0\tilde{\chi}_{\text{em},n}^\ell * \tilde{H}_{\text{av},n}^\ell\right), \tag{B4b}$$

where Δ and the subscript "av" refer to the difference and average of the spectral coefficients, respectively (e.g., $\Delta\tilde{E}_n^\ell = \tilde{E}_n^\ell(\rho_\ell) - \tilde{E}_n^{\ell+1}(\rho_\ell)$, and $\tilde{E}_{\text{av},n}^\ell = [\tilde{E}_n^\ell(\rho_\ell) + \tilde{E}_n^{\ell+1}(\rho_\ell)]/2$) and the asterisk ("$*$") denotes a discrete convolution product with respect to n. Equation (B4) forms a set of $2L(2N+1)$ equations with $2L(2N+1)$ unknown, the expansion coefficients a_n^ℓ and b_n^ℓ in Eq. (B1). Note that since the number of regions is $L+1$, the number of expansion modes is $(2N+1)$, and there are two coefficients per region, the number of expansion coefficients is $2(L+1)(2N+1)$, which is greater than the size of the matrix system, $2L(2N+1)$. However, b_n^1 and a_n^{L+1} are known quantities: For external (plane-wave) illumination, $b_n^1 \neq 0$ and $a_n^{L+1} = 0$, while for internal (point-source) illumination, $b_n^1 = 0$ and $a_n^{L+1} \neq 0$. Thus, the number of *unknown* coefficients is really $2L(2N+1)$, corresponding to the size of the matrix system.

1. External illumination

In this case,

$$b_n^1 = 1 \tag{B5a}$$

and

$$a_n^{L+1} = 0, \tag{B5b}$$

where $b_n^1 \neq 0$ $(\forall n)$ corresponds to the expansion of the (assumed) incident plane wave in cylindrical wave functions [28] and $a_n^{L+1} = 0$ $(\forall n)$ corresponds to the absence of internal illumination.

Inserting Eq. (B2) into Eq. (B4) leads to the following matrix equation,

$$\begin{pmatrix}
\mathbf{P}_{\mathbf{a}^1}^{\rho_1} & \mathbf{P}_{\mathbf{a}^2}^{\rho_1} & \mathbf{P}_{\mathbf{b}^2}^{\rho_1} & \mathbf{0} & \mathbf{0} & \cdots & \mathbf{0} & \mathbf{0} & \mathbf{0} \\
\mathbf{Q}_{\mathbf{a}^1}^{\rho_1} & \mathbf{Q}_{\mathbf{a}^2}^{\rho_1} & \mathbf{Q}_{\mathbf{b}^2}^{\rho_1} & \mathbf{0} & \mathbf{0} & \cdots & \mathbf{0} & \mathbf{0} & \mathbf{0} \\
\mathbf{0} & \mathbf{P}_{\mathbf{a}^2}^{\rho_2} & \mathbf{P}_{\mathbf{b}^2}^{\rho_2} & \mathbf{P}_{\mathbf{a}^3}^{\rho_2} & \mathbf{P}_{\mathbf{b}^3}^{\rho_2} & \cdots & \mathbf{0} & \mathbf{0} & \mathbf{0} \\
\mathbf{0} & \mathbf{Q}_{\mathbf{a}^2}^{\rho_2} & \mathbf{Q}_{\mathbf{b}^2}^{\rho_2} & \mathbf{Q}_{\mathbf{a}^3}^{\rho_2} & \mathbf{Q}_{\mathbf{b}^3}^{\rho_2} & \cdots & \mathbf{0} & \mathbf{0} & \mathbf{0} \\
\vdots & \vdots & \vdots & \vdots & \vdots & \ddots & \vdots & \vdots & \vdots \\
\mathbf{0} & \mathbf{0} & \mathbf{0} & \mathbf{0} & \mathbf{0} & \cdots & \mathbf{P}_{\mathbf{a}^L}^{\rho_L} & \mathbf{P}_{\mathbf{b}^L}^{\rho_L} & \mathbf{P}_{\mathbf{b}^{L+1}}^{\rho_L} \\
\mathbf{0} & \mathbf{0} & \mathbf{0} & \mathbf{0} & \mathbf{0} & \cdots & \mathbf{Q}_{\mathbf{a}^L}^{\rho_L} & \mathbf{Q}_{\mathbf{b}^L}^{\rho_L} & \mathbf{Q}_{\mathbf{b}^{L+1}}^{\rho_L}
\end{pmatrix}
\times \begin{pmatrix} \mathbf{a}^1 \\ \mathbf{a}^2 \\ \mathbf{b}^2 \\ \mathbf{a}^3 \\ \mathbf{b}^3 \\ \vdots \\ \mathbf{a}^L \\ \mathbf{b}^L \\ \mathbf{b}^{L+1} \end{pmatrix}
= \begin{pmatrix} -\mathbf{P}_{\mathbf{b}^1}^{\rho_1}\,\mathbb{1} \\ -\mathbf{Q}_{\mathbf{b}^1}^{\rho_1}\,\mathbb{1} \\ \mathbb{O} \\ \mathbb{O} \\ \vdots \\ \mathbb{O} \\ \mathbb{O} \end{pmatrix}, \tag{B6}$$

which involves the $(2N+1)\times 1$ vectors:

$$\mathbf{a}^{\ell}=\begin{pmatrix} a^{\ell}_{-N}\\ \vdots \\ a^{\ell}_{N}\end{pmatrix}, \tag{B7a}$$

$$\mathbf{b}^{\ell}=\begin{pmatrix} b^{\ell}_{-N}\\ \vdots \\ b^{\ell}_{N}\end{pmatrix}, \tag{B7b}$$

containing the unknown expansion coefficients a_n^{ℓ} and b_n^{ℓ}, and the $(2N+1)\times(2N+1)$ coefficient matrices

$$\mathbf{P}^{\rho_\ell}_{\mathbf{a}^\ell}=\left(1-j\frac{k_0}{2}\tilde{\boldsymbol{\chi}}^{\ell}_{\text{me}}\right)\mathbf{H}^{\rho_\ell}_{k_\ell}-\frac{k_0\eta_0}{2\eta_\ell}\tilde{\boldsymbol{\chi}}^{\ell}_{\text{mm}}\mathbf{H}'^{\rho_\ell}_{k_\ell}, \tag{B8a}$$

$$\mathbf{P}^{\rho_\ell}_{\mathbf{b}^\ell}=\left(1-j\frac{k_0}{2}\tilde{\boldsymbol{\chi}}^{\ell}_{\text{me}}\right)\mathbf{J}^{\rho_\ell}_{k_\ell}-\frac{k_0\eta_0}{2\eta_\ell}\tilde{\boldsymbol{\chi}}^{\ell}_{\text{mm}}\mathbf{J}'^{\rho_\ell}_{k_\ell}, \tag{B8b}$$

$$\mathbf{P}^{\rho_\ell}_{\mathbf{a}^{\ell+1}}=\left(-1-j\frac{k_0}{2}\tilde{\boldsymbol{\chi}}^{\ell}_{\text{me}}\right)\mathbf{H}^{\rho_\ell}_{k_{\ell+1}}-\frac{k_0\eta_0}{2\eta_{\ell+1}}\tilde{\boldsymbol{\chi}}^{\ell}_{\text{mm}}\mathbf{H}'^{\rho_\ell}_{k_{\ell+1}}, \tag{B8c}$$

$$\mathbf{P}^{\rho_\ell}_{\mathbf{b}^{\ell+1}}=\left(-1-j\frac{k_0}{2}\tilde{\boldsymbol{\chi}}^{\ell}_{\text{me}}\right)\mathbf{J}^{\rho_\ell}_{k_{\ell+1}}-\frac{k_0\eta_0}{2\eta_{\ell+1}}\tilde{\boldsymbol{\chi}}^{\ell}_{\text{mm}}\mathbf{J}'^{\rho_\ell}_{k_{\ell+1}}, \tag{B8d}$$

$$\mathbf{Q}^{\rho_\ell}_{\mathbf{a}^\ell}=\frac{\eta_0}{\eta_\ell}\left(1-j\frac{k_0}{2}\tilde{\boldsymbol{\chi}}^{\ell}_{\text{em}}\right)\mathbf{H}'^{\rho_\ell}_{k_\ell}+\frac{k_0}{2}\tilde{\boldsymbol{\chi}}^{\ell}_{\text{ee}}\mathbf{H}^{\rho_\ell}_{k_\ell}, \tag{B8e}$$

$$\mathbf{Q}^{\rho_\ell}_{\mathbf{b}^\ell}=\frac{\eta_0}{\eta_\ell}\left(1-j\frac{k_0}{2}\tilde{\boldsymbol{\chi}}^{\ell}_{\text{em}}\right)\mathbf{J}'^{\rho_\ell}_{k_\ell}+\frac{k_0}{2}\tilde{\boldsymbol{\chi}}^{\ell}_{\text{ee}}\mathbf{J}^{\rho_\ell}_{k_\ell}, \tag{B8f}$$

$$\mathbf{Q}^{\rho_\ell}_{\mathbf{a}^{\ell+1}}=-\frac{\eta_0}{\eta_{\ell+1}}\left(1+j\frac{k_0}{2}\tilde{\boldsymbol{\chi}}^{\ell}_{\text{em}}\right)\mathbf{H}'^{\rho_\ell}_{k_{\ell+1}}+\frac{k_0}{2}\tilde{\boldsymbol{\chi}}^{\ell}_{\text{ee}}\mathbf{H}^{\rho_\ell}_{k_{\ell+1}}, \tag{B8g}$$

and

$$\mathbf{Q}^{\rho_\ell}_{\mathbf{b}^{\ell+1}}=-\frac{\eta_0}{\eta_{\ell+1}}\left(1+j\frac{k_0}{2}\tilde{\boldsymbol{\chi}}^{\ell}_{\text{em}}\right)\mathbf{J}'^{\rho_\ell}_{k_{\ell+1}}+\frac{k_0}{2}\tilde{\boldsymbol{\chi}}^{\ell}_{\text{ee}}\mathbf{J}^{\rho_\ell}_{k_{\ell+1}}, \tag{B8h}$$

which involve the $(2N+1)\times(2N+1)$ Toeplitz susceptibility matrix

$$\tilde{\boldsymbol{\chi}}^{\ell}_{pq}=\begin{pmatrix} \tilde{\chi}^{\ell}_{pq,0} & \tilde{\chi}^{\ell}_{pq,-1} & \cdots & \tilde{\chi}^{\ell}_{pq,-2N}\\ \tilde{\chi}^{\ell}_{pq,1} & \tilde{\chi}^{\ell}_{pq,0} & \cdots & \tilde{\chi}^{\ell}_{pq,-2N+1}\\ \vdots & \vdots & \ddots & \vdots\\ \tilde{\chi}^{\ell}_{pq,2N} & \tilde{\chi}^{\ell}_{pq,2N-1} & \cdots & \tilde{\chi}^{\ell}_{pq,0}\end{pmatrix}, \tag{B9a}$$

where $p,q=e,m$, the $(2N+1)\times(2N+1)$ diagonal Hankel and Bessel functions and their derivative matrices

$$\mathbf{H}^{\rho_\ell}_{k_\ell}=\text{diag}\left(H_n^{(2)}(k_\ell\rho_\ell)\right), \tag{B9b}$$

$$\mathbf{H}'^{\rho_\ell}_{k_\ell}=\text{diag}\left(H_n^{(2)\prime}(k_\ell\rho_\ell)\right), \tag{B9c}$$

$$\mathbf{J}^{\rho_\ell}_{k_\ell}=\text{diag}\left(J_n(k_\ell\rho_\ell)\right), \tag{B9d}$$

$$\mathbf{J}'^{\rho_\ell}_{k_\ell}=\text{diag}\left(J'_n(k_\ell\rho_\ell)\right), \tag{B9e}$$

the $(2N+1)\times 1$ identity and zero vectors $\mathbb{1}$ and $\mathbb{O}$, respectively, and the $(2N+1)\times(2N+1)$ zero matrix $\mathbf{0}$. It may easily be verified that the coefficient matrix in Eq. (B6) has the dimension $2L(2N+1)\times 2L(2N+1)$. Note that the coefficient matrix is a diagonal-band matrix because only $a_\ell, b_\ell, a_{\ell+1}$ and $b_{\ell+1}$ contribute in the GSTCs in Eq. (B4) for each metasurface ℓ.

2. Internal illumination

In this case,

$$b_n^1=0 \tag{B10a}$$

and

$$a_n^{L+1}=-j^n\frac{k_{L+1}\eta_{L+1}}{4}J_n\left(k_{L+1}\rho'\right)e^{-jn\phi'}, \tag{B10b}$$

where $b_n^1=0$ $(\forall n)$ corresponds to the absence of external illumination and $a_n^{L+1}\neq 0$ $(\forall n)$ corresponds to the circular-cylindrical wave expansion of the radiated fields of an off-center line source placed at the polar coordinates (ρ',ϕ') (see Ref. [38]).

Equation (B4) leads to the same matrix system as for the case of external illumination, namely Eq. (B6), but with the input vector on the right-hand side of the equation replaced by

$$\begin{pmatrix} \mathbb{O}\\ \mathbb{O}\\ \mathbb{O}\\ \mathbb{O}\\ \vdots\\ -\mathbf{P}^{\rho_L}_{\mathbf{a}^{L+1}}\,\boldsymbol{\kappa}\\ -\mathbf{Q}^{\rho_L}_{\mathbf{a}^{L+1}}\,\boldsymbol{\kappa}\end{pmatrix}, \tag{B11}$$

where $\boldsymbol{\kappa}=\mathbf{a}^{L+1}$.

[1] U. Leonhardt, Optical conformal mapping, Science **312**, 1777 (2006).

[2] J. B. Pendry, D. Schurig, and D. R. Smith, Controlling electromagnetic fields, Science **312**, 1780 (2006).

[3] R. Fleury, F. Monticone, and A. Alù, Invisibility and Cloaking: Origins, Present, and Future Perspectives, Phys. Rev. Appl. **4**, 037001:1 (2015).

[4] D. Schurig, J. J. Mock, B. J. Justice, S. A. Cummer, J. B. Pendry, A. F. Starr, and D. R. Smith, Metamaterial electromagnetic cloak at microwave frequencies, Science **314**, 977 (2006).

[5] A. Alù and N. Engheta, Achieving transparency with plasmonic and metamaterial coatings, Phys. Rev. E **72**, 016623 (2005).

[6] M. G. Silveirinha, A. Alù, and N. Engheta, Parallel-plate metamaterials for cloaking structures, Phys. Rev. E **75**, 036603 (2007).

[7] P. Alitalo and S. Tretyakov, Electromagnetic cloaking with metamaterials, Mater. Today **12**, 22 (2009).

[8] M. Selvanayagam and G. V. Eleftheriades, Experimental Demonstration of Active Electromagnetic Cloaking, Phys. Rev. X **3**, 041011 (2013).

[9] M. Dehmollaian and C. Caloz, in *Fifteenth Int. Congr. Art. Mat. Nov. Wave. Phenom. (Metamaterials'2021)* (New York, 2021), p. 111.

[10] H. Lee and D.-H. Kwon, Microwave Metasurface Cloaking for Freestanding Objects, Phys. Rev. Appl. **17**, 054012 (2022).

[11] H. A. Lorentz, The theorem of Poynting concerning the energy in the electromagnetic field and two general propositions concerning the propagation of light, Amsterdammer Akademie der Wetenschappen **4**, 1 (1896).

[12] C. He, X.-L. Zhang, L. Feng, M.-H. Lu, and Y. Chen, One-way cloak based on nonreciprocal photonic crystal, Appl. Phys. Lett. **99**, 151112 (2011).

[13] X. Zhu, L. Feng, P. Zhang, X. Yin, and X. Zhang, One-way invisible cloak using parity-time symmetric transformation optics, Opt. Lett. **38**, 2821 (2013).

[14] D. L. Sounas, R. Fleury, and A. Alù, Unidirectional Cloaking Based on Metasurfaces with Balanced Loss and Gain, Phys. Rev. Appl. **4**, 014005 (2015).

[15] G. Lavigne, K. Achouri, V. S. Asadchy, S. A. Tretyakov, and C. Caloz, Susceptibility derivation and experimental demonstration of refracting metasurfaces without spurious diffraction, IEEE Trans. Antennas Propag. **66**, 1321 (2018).

[16] K. Achouri and C. Caloz, *Electromagnetic Metasurfaces: Theory and Applications* (John Wiley & Sons, Hoboken, NJ, 2021).

[17] G. Lavigne, T. Kodera, and C. Caloz, Metasurface magnetless specular isolator, Sci. Rep. **12**, 1 (2022).

[18] C. Caloz, A. Alù, S. Tretyakov, D. Sounas, K. Achouri, and Z.-L. Deck-Léger, Electromagnetic Nonreciprocity, Phys. Rev. Appl. **10**, 047001:1 (2018).

[19] S. Taravati, B. S. Khan, S. Gupta, K. Achouri, and C. Caloz, Nonreciprocal nongyrotropic magnetless metasurface, IEEE Trans. Antennas Propag. **65**, 3589 (2017).

[20] As with all cloaks, this cloaking system is subjected to a fundamental trade-off between cloaking efficiency (minimal scattering) and its operation bandwidth, due to the physical impossibility (or impracticality [39]) of the deflected part of the energy near the center propagating superluminally for proper phase synchronization with the undeflected part of the energy in the periphery [40].

[21] G. Lavigne and C. Caloz, Magnetless reflective gyrotropic spatial isolator metasurface, New J. Phys. **23**, 1 (2021).

[22] S. Taravati and G. V. Eleftheriades, Full-duplex reflective beamsteering metasurface featuring magnetless nonreciprocal amplification, Nat. Commun. **12**, 1 (2021).

[23] Y. Shi, S. Han, and S. Fan, Optical circulation and isolation based on indirect photonic transitions of guided resonance modes, ACS Photonics **4**, 1639 (2017).

[24] S. Taravati and G. V. Eleftheriades, Full-Duplex Nonreciprocal Beam Steering by Time-Modulated Phase-Gradient Metasurfaces, Phys. Rev. Appl. **14**, 014027 (2020).

[25] M. Idemen and A. H. Serbest, Boundary conditions of the electromagnetic field, Electron. Lett. **13**, 704 (1987).

[26] E. F. Kuester, M. A. Mohamed, M. Piket-May, and C. L. Holloway, Averaged transition conditions for electromagnetic fields at a metafilm, IEEE Trans. Antennas Propag. **51**, 2641 (2003).

[27] K. Achouri, M. A. Salem, and C. Caloz, General metasurface synthesis based on susceptibility tensors, IEEE Trans. Antennas Propag. **63**, 2977 (2015).

[28] R. Harrington, *Time Harmonic Electromagnetic Fields* (Wiley–IEEE Press, New York, NY, 2001).

[29] A. Ishimaru, *Electromagnetic Wave Propagation, Radiation, and Scattering* (Wiley–IEEE Press, Hoboken, NJ, 2017).

[30] C. A. Balanis, *Antenna Theory: Analysis and Design* (John Wiley & Sons, Hoboken, NJ, 2016).

[31] B. P. Lathi, *Modern Digital and Analog Communication Systems* (Oxford University Press, New York, NY, 1995).

[32] B. E. Saleh and M. C. Teich, *Fundamentals of Photonics* (John Wiley & Sons, Hoboken, NJ, 2019).

[33] X. Wang and C. Caloz, Spread-spectrum selective camouflaging based on time-modulated metasurface, IEEE Trans. Antennas Propag. **69**, 286 (2021).

[34] N. Lebbe, S. Lanteri, S. Y. Golla, and P. Genevet, Susceptibility synthesis of arbitrary shaped metasurfaces, Phys. Rev. B **106**, 035110 (2022).

[35] N. Chamanara, Y. Vahabzadeh, and C. Caloz, Simultaneous control of the spatial and temporal spectra of light with space-time varying metasurfaces, IEEE Trans. Antennas Propag. **67**, 2430 (2019).

[36] K. Zhou, W. Li, B. B. Patel, R. Tao, Y. Chang, S. Fan, Y. Diao, and L. Cai, Three-dimensional printable nanoporous polymer matrix composites for daytime radiative cooling, Nano Lett. **21**, 1493 (2021).

[37] M. Dehmollaian, G. Lavigne, and C. Caloz, Comparison of tensor boundary conditions (TBCs) with generalized sheet transition conditions (gstcs), IEEE Trans. Antennas Propag. **67**, 7396 (2019).

[38] D. G. Dudley, *Mathematical Foundations for Electromagnetic Theory* (IEEE Press, New York, 1994).

[39] J. D. Jackson, Classical electrodynamics (John Wiley & Sons, Hoboken, NJ, 1999).

[40] D. A. Miller, On perfect cloaking, Opt. Express **14**, 12457 (2006).